

## Energies and lifetimes of atomic Rydberg states near metal surfaces

P. Nordlander

*Department of Physics and Rice Quantum Institute, Rice University, Houston, Texas 77251*

(Received 30 May 1995)

The energy shifts and broadenings of atomic Rydberg states have been calculated as a function of distance from a metal surface using the complex scaling technique. The results of this calculation show a relatively complicated distance dependence of the energy shifts and broadenings of the levels near the surface. Some of the orbitals hybridize with each other, resulting in states with wave functions that differ strongly in their orientation with respect to the surface. The widths of the states oriented toward the metal are found to be many orders of magnitude broader than the states oriented toward the vacuum. The widths of some states exhibit a nonexponential dependence on atom-surface separation. It is shown that for an accurate description of the interaction of Rydberg atoms with metal surfaces it is important to employ a realistic surface potential.

### I. INTRODUCTION

The interaction of highly excited Rydberg atoms with surfaces is of considerable scientific interest. Rydberg atoms are relatively simple systems with properties that derive from basic physical principles rather than complicated chemistry. Of particular interest is the study of charge transfer processes between highly excited Rydberg states and metal surfaces. Due to the large spatial extent of highly excited states, charge transfer reactions occur at large distances from the surface. In this region, the surface potential is believed to be relatively simple in character.

Resonant transfer of electrons between the conduction-band and high-lying ionic Rydberg states is usually the dominant electronic process in the scattering of slow, highly charged ions by metal surfaces.<sup>1</sup> The formation of highly excited hydrogen ( $n \leq 10$ ) atoms has been observed in low-energy ion-surface collisions.<sup>2-4</sup> The ionization of Rydberg atoms outside metal surfaces has been studied using mesh transmission experiments.<sup>5-7</sup> Recently an experimental approach for the measurement of the ionization distances of Rydberg atoms near metal surfaces has been developed.<sup>8</sup>

The probability for electron transfer between a Rydberg atom and a metal surface has been previously investigated theoretically. By using an approximate analogy between the atom-surface interaction problem and the Stark problem when the atom is far from the surface, the shifts and widths of atomic Rydberg levels were estimated for asymptotic distances.<sup>9</sup> The interaction of Rydberg atoms with the surface have recently been studied extensively by Wille using perturbation theory.<sup>10-12</sup> In this work, the surface was modeled using a finite barrier model neglecting the image interaction between the electron and the surface. Furthermore, the calculations were performed using an unperturbed atomic basis neglecting the surface-induced hybridization of the atomic orbitals. While this approach would be valid for large atom-surface separations and for highly charged ions, these approximations are questionable for neutral Rydberg atoms at thermal energies.

In this paper, we present a first-principles calculation of the energy-level shift and broadening of atomic Rydberg levels outside a metal surface as a function of atom-surface

separation. The energy shift and broadening are obtained directly from the surface potential using the complex scaling method.<sup>13</sup> The surface is described using a density-functional method that properly includes the image potential. The surface-induced hybridization of the atomic levels is properly included.

The results of the calculation show a relatively complicated distance dependence of the energy shift and broadening of atomic Rydberg levels near the surface. It is shown that some of the levels hybridize strongly with each other, resulting in states with a pronounced orientation. For intermediate atom-surface separations, the states oriented toward the surface are shown to shift downward with decreasing atom-surface separation. Due to the distance dependence of the hybridization, some level widths exhibit a nonexponential dependence on the atom-surface separation. The widths of the hybridized states oriented toward the metal are found to be many orders of magnitude broader than the states oriented toward the vacuum. The hybridization of the atomic orbitals is found to depend sensitively on details of the surface potential. For an accurate description of the energy shifts and broadenings of atomic Rydberg states near metal surfaces it is therefore necessary to employ a realistic surface potential.

In Sec. II, some theoretical details of the calculation are described. In Sec. III, the results are presented. In Sec. IV, the results are compared with results from a calculation employing the finite barrier model for the surface. In Sec. V, the conclusions are outlined.

### II. THEORY

The broadenings and shifts of atomic levels near the surface are induced by the surface electron potential. In Sec. II A, a method for the calculation of the surface electron potential is presented. In Sec. II B, our method for calculating the energies and broadenings of the atomic resonances is discussed.

#### A. Electron potential outside surfaces

Although the basic features of the surface potential can be understood from a simple image model, such an approxima-

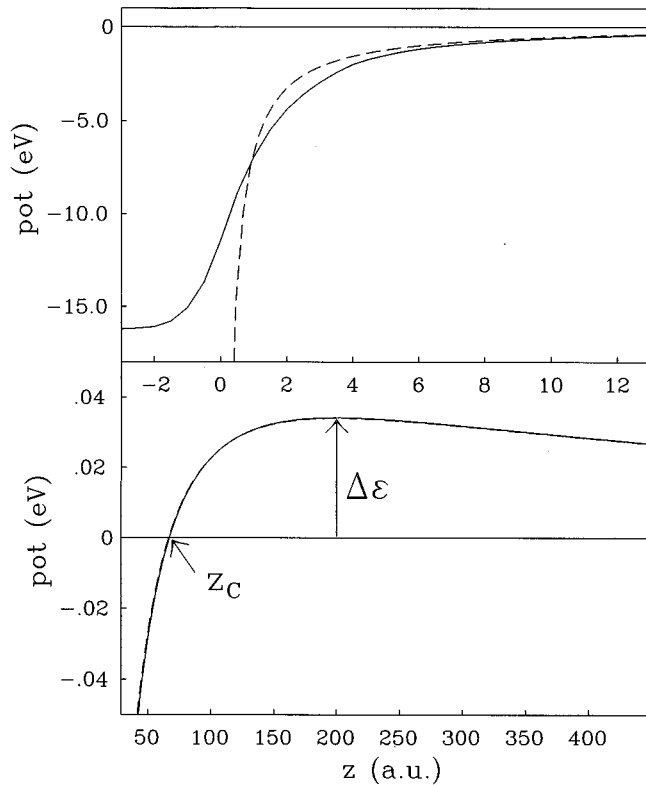


FIG. 1. Calculated surface potential  $\Delta V^{\text{surf}}(\rho, z; Z)$  as a function of  $z$  for  $\rho=0$  and  $Z=200$  a.u. The distances  $z$  and  $Z$  refer to the jellium edge. Positive  $z$  and  $Z$  are in the vacuum direction. The solid lines are the results obtained using the density-functional method and the dashed lines are results obtained assuming a perfectly conducting metal surface using a simple image model. The upper panel shows the potential near the surface and the lower panel shows the potential for large  $z$ . The quantities  $\Delta\epsilon$  and  $z_c$  are defined in the text. The jellium is characterized by  $r_s=2$ .

tion would be too crude for the evaluation of tunneling probabilities between atoms and surfaces.<sup>13</sup> To model the surface we invoke the jellium model,<sup>14</sup> and use cylindrical coordinates with the cylinder axis through the hydrogen atom. The electron coordinates are denoted  $(\rho, z, \alpha)$  and uppercase letters  $Z$  refer to the atomic coordinates. The distances  $z$  and  $Z$  refer to the jellium edge. Positive distances are in the vacuum direction. Atomic units will be used throughout the text unless otherwise indicated.

In this calculation, a one-electron description will be assumed. This approximation is reasonable for the description of one-electron events such as resonant tunneling between the ion and the solid but does not describe two-electron events such as Auger deexcitation which may be important close to the surface (for atom-surface separations  $Z < 5$  a.u.). The atom-surface separations considered in this paper are far from the surface ( $Z > 50$  a.u.) and many-electron effects can therefore safely be neglected.

The total potential for the electron at coordinates  $(\rho, z)$  can be written as

$$V^{\text{eff}}(\rho, z; Z) = V_0^s(z) + \Delta V_A^s(\rho, z; Z). \quad (1)$$

The first part of the potential  $V_0^s(z)$  describes the bare

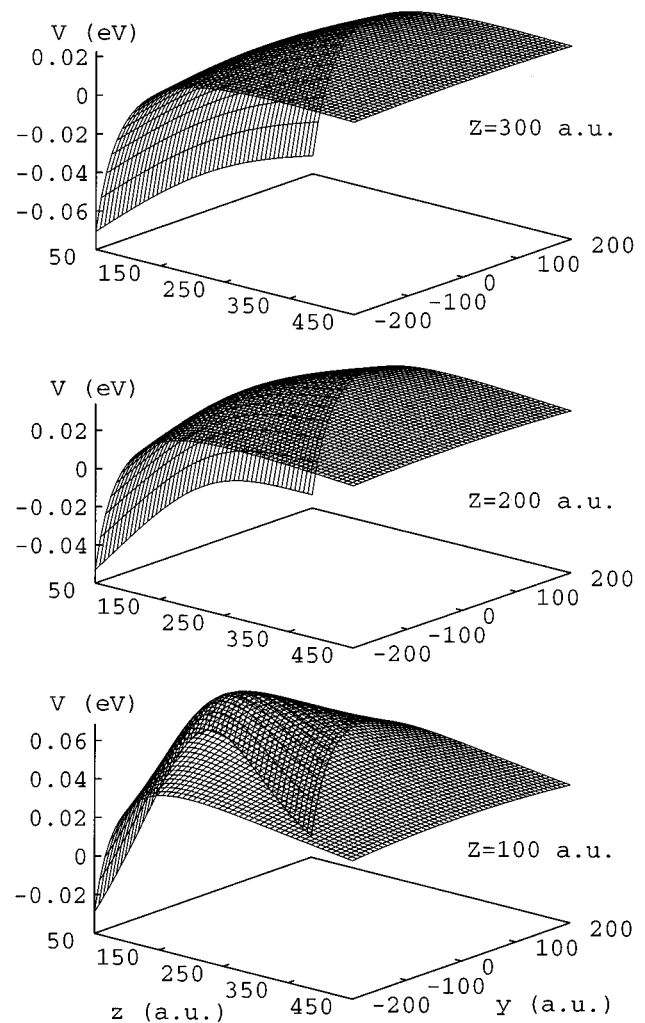


FIG. 2. Calculated surface potential  $\Delta V^{\text{surf}}(\rho, z; Z)$  as a function of  $z$  and  $\rho$  for three different proton-surface separations. For illustrative purposes, the potential is shown as a function of lateral coordinate  $y$  where  $\rho=|y|$ . The upper panel is for  $Z=300$  a.u., the middle panel is for  $Z=200$  a.u., and the lower panel is for  $Z=100$  a.u. The jellium is characterized by  $r_s=2$ .

electron-surface interaction. The second term,  $\Delta V_A^s$ , describes the surface potential induced by the proton.

There exist several first-principles schemes for the calculation of the one-electron potential,  $V_0^s(z)$ , outside metal surfaces. To properly describe electron tunneling between a surface and an atom it is important to use a potential that includes image effects.<sup>13</sup> In the present case we have adopted the weighted density approximation.<sup>15,16</sup> This particular many-body approach describes both the image interaction and the potential in the bulk. For large  $z$ ,  $V_0^s(z) \rightarrow -1/4(z - z_{\text{im}})$ , where  $z_{\text{im}}$  is the image plane defined as the first moment of the charge distribution induced by an external electric field.<sup>17</sup>

The  $\Delta V_A^s(\rho, z; Z)$  term describes how the bare surface electron potential is modified when the proton is present. There are two contributions to this term: the direct Coulomb potential from the proton and the potential from the proton-

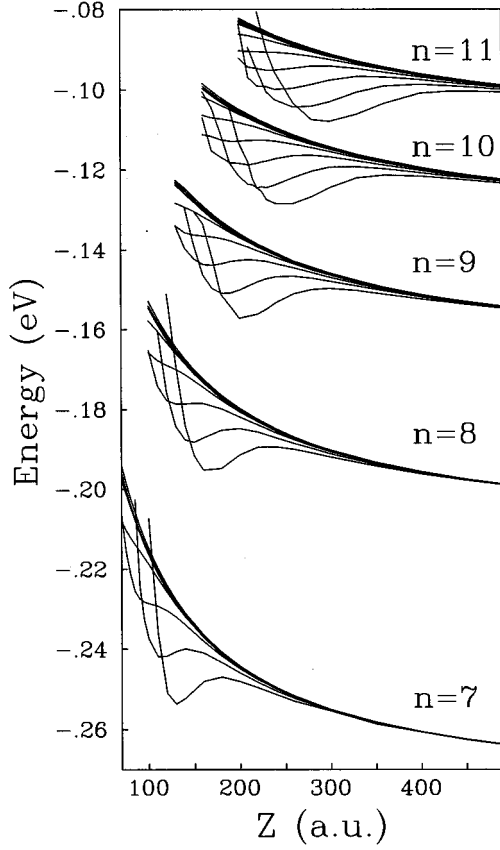


FIG. 3. Calculated energy shifts of the  $H(n=7-11)$   $m=0$  states as a function of distance  $Z$  outside a jellium surface ( $r_s=2$ ).

induced image charge in the surface. For large electron-surface separations  $z$  and atom-surface separations  $Z$ , the latter contribution approaches its classical value  $1/\sqrt{\rho^2 + (z+Z-2z_{\text{im}})^2}$ . For intermediate separations, the image contribution is estimated using a linear response approach. Theoretical studies have shown that the surface charges induced by a moderate external perturbation are distributed in a relatively thin layer in the surface region. The thickness of this layer  $\Delta$  as well as the location  $z_{\text{im}}$  depends on the  $r_s$  of the metal.<sup>17</sup>

We assume that the proton-induced image surface charge distribution can be written as

$$\sigma(\rho', z', Z) = \frac{1}{\sqrt{\Delta\pi}} \exp\left[-\left(\frac{z' - z_{\text{im}}}{\Delta}\right)^2\right] \sigma_{\text{cl}}(\rho', Z - z_{\text{im}}), \quad (2)$$

where  $\sigma_{\text{cl}}$  is the classical surface charge density induced on a perfectly conducting metal surface by a unit charge at a distance  $Z - z_{\text{im}}$ . The primed coordinates  $z'$  and  $\rho'$  here refer to the induced electron density distribution along the surface. Using this ansatz for  $\sigma$ , the change in the electrostatic potential as well as the induced exchange-correlation potential can be calculated using Poisson's equation and a proper exchange-correlation functional.<sup>18</sup>

In order to understand the effects of the surface on the atomic levels it is useful to subtract the Coulomb potential between the electron and the proton from the effective potential given in Eq. (1),

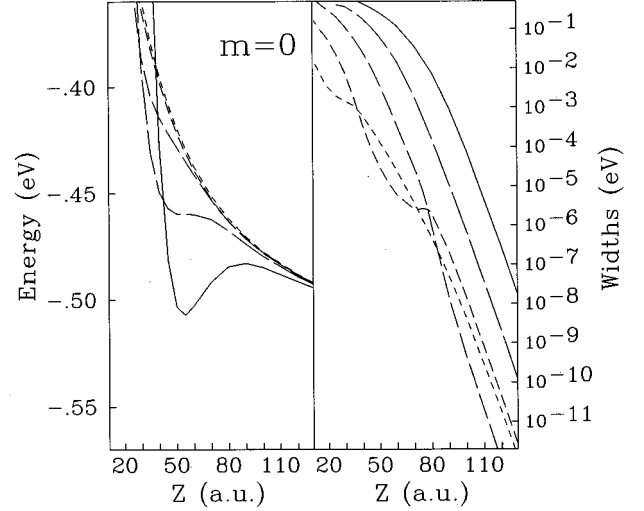


FIG. 4. Calculated energy shifts (left) and widths (right) as a function of distance of the five  $H(n=5, m=0)$  states outside a jellium surface ( $r_s=2$ ). The five different states are drawn with different dashed patterns. The same dashed pattern is used both for the real part and the imaginary part of the atomic state.

$$\Delta V^{\text{surf}}(\rho, z; Z) = V^{\text{eff}}(\rho, z; Z) + \frac{1}{r}. \quad (3)$$

This quantity is the difference between the one-electron potential when the atom is near the surface and when the atom is in vacuum. In a perturbative calculation of the shifts and broadenings of the atomic levels,  $\Delta V^{\text{surf}}$  would be the perturbing potential.

In Fig. 1, we show  $\Delta V^{\text{surf}}(\rho, z; Z)$  as a function of  $z$  along the surface normal through the proton, i.e., for  $\rho=0$ . The upper panel shows the surface potential close to the surface and the lower panel shows the potential on a larger scale. For comparison, we also show the potential obtained assuming that the surface is a perfect conductor. The difference between the density-functional potential and the classical potential is largest for small  $z$ . For small  $z$ , the jellium potential saturates and reaches its bulk value within a few a.u. from the jellium edge. The classical image potential varies more strongly with  $z$  and diverges at  $z=0$ . For large  $z$ , the difference between the density-functional potential and the classical image potential becomes negligible. From Fig. 1, it can be seen that the surface-induced potential is negative for  $z < z_c$ , and is positive in a region  $z > z_c$ . The surface potential has a maximum  $\Delta\epsilon(Z) = \Delta V^{\text{surf}}(0, Z; Z)$  for  $z=Z$ , and vanishes as  $z \rightarrow \infty$ . In a classical image model,  $\Delta\epsilon(Z) = 27.2/4Z$  eV and  $z_c = Z/3$ . The corresponding values of  $\Delta\epsilon(Z)$  and  $z_c$  for the density-functional potential are similar. Since the surface potential is positive and approximately equal to  $\Delta\epsilon(Z)$  in an extended region around the proton, localized atomic states are expected to shift upward by an amount  $\approx \Delta\epsilon(Z)$ . As will be demonstrated in Sec. III, highly excited Rydberg states can sometimes extend into the region  $z < z_c$  and therefore lower their energy. The degree to which this happens depends on the surface-induced hybridization of the degenerate Rydberg orbitals. For a correct description of this hybridization it is crucial to use the proper surface potential.<sup>13</sup>

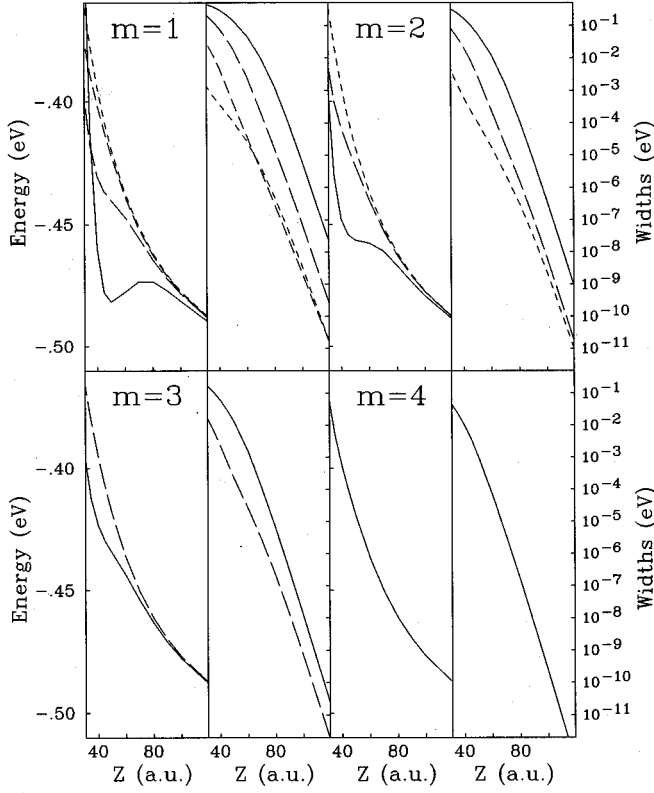


FIG. 5. Calculated energy shifts (left) and widths (right) as a function of distance of H( $n=5$ ),  $m=1-4$  outside a jellium surface ( $r_s=2$ ). The different states for each  $m$  are drawn with different dashed patterns. The same dashed pattern is used both for the real part and the imaginary part of the atomic state.

In Fig. 2, we show  $\Delta V^{\text{surf}}(\rho, z; Z)$  for three different atom-surface separations  $Z$ . It can be seen that the topology of the potential is relatively complicated. Near the surface, the image interaction between the electron and the metal dominates the potential and results in a strong attraction. For large  $z$ , the surface potential is small and varies relatively weakly with  $z$ . The lateral variation of the surface potential depends on both  $z$  and  $Z$ . The lateral variations are always largest for small  $z$ . For small  $Z$ , the surface potential shows a strong  $\rho$  dependence in the region close to the surface. For large  $Z$ , the  $\rho$  dependence becomes weaker.

### B. Calculations of the shifts and broadenings of atomic levels near surfaces

When an atom comes close to a metal surface, the probability for resonant tunneling of electrons between the atom and the surface increases. Some of the atomic levels thereby become resonances. This fact complicates the description of the levels significantly. In order to calculate the level shifts and broadenings, the Schrödinger equation for the electrons must be solved:

$$\left[ -\frac{1}{2} \nabla^2 + V^{\text{eff}}(\rho, z; Z) \right] \psi = \epsilon \psi \quad (4)$$

under resonance boundary conditions:

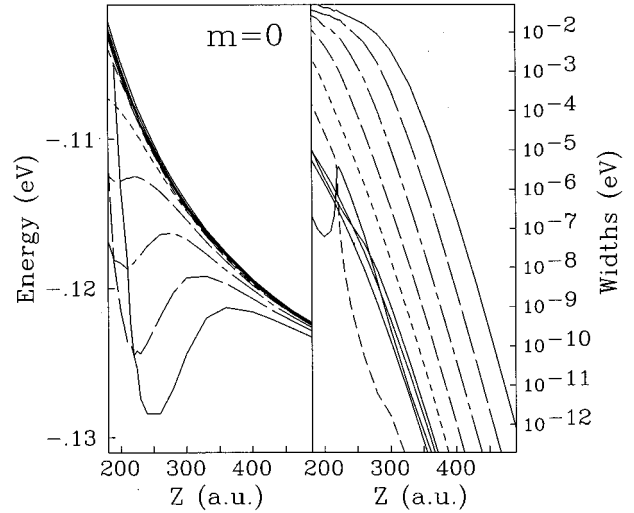


FIG. 6. Calculated energy shifts (left) and widths (right) as a function of distance of H( $n=10$ ),  $m=0$  outside a jellium surface ( $r_s=2$ ). The different states are drawn with different dashed patterns. The same dashed pattern is used both for the real part and the imaginary part of the atomic state.

$$\psi(r) \rightarrow \frac{1}{r} e^{ik_R r + k_I r} f(\Omega), \quad (5)$$

where  $k_I$  is positive. The energy is related to the complex wave number  $k$  through  $\epsilon = -(1/2)(k_R + ik_I)^2$ . The energy thus becomes complex,  $\epsilon = \epsilon_R - i\epsilon_I$ . The real part of the energy,  $\epsilon_R$ , describes the energy of the level and the imaginary part,  $\epsilon_I$ , describes the half-width of the resonance. Since  $V^{\text{eff}}$  depends explicitly on the atom-surface separation  $Z$ , both  $\epsilon_R$  and  $\epsilon_I$  will depend on  $Z$ .

Resonances can be directly obtained from Eq. (4) by extending the coordinates to the complex plane. A convenient method for this is the complex scaling method.<sup>13,19-22</sup> The idea is to introduce a complex variable substitution in the atomic radial coordinate,  $r \rightarrow \exp[i\alpha]r$ . Upon this variable transformation, the resonance boundary condition is changed to

$$\Psi(r) \rightarrow e^{i(k_R \cos \alpha + k_I \sin \alpha)r + (k_I \cos \alpha - k_R \sin \alpha)r}. \quad (6)$$

If  $\alpha$  is chosen larger than  $\arctan k_I/k_R$  this expression vanishes asymptotically. This means that the resulting Hamiltonian can be diagonalized using a normalizable basis. The advantage of simpler boundary conditions is at the expense of having to invert a complex non-Hermitian Hamiltonian. This lengthens the computation time somewhat but is not a serious problem.

For a jellium surface, there is no azimuthal dependence of the surface potential. The atomic wave functions are expanded in a finite basis set consisting of generalized Laguerre polynomials,

$$\phi_{nlm} = \exp\left[-\frac{\lambda r}{2}\right] r^{l+1} L_n^{2l+2}(\lambda r) Y_{lm}(\Omega). \quad (7)$$

In this expression,  $L_n^{2l+2}$  is a generalized Laguerre polynomial and  $Y_{lm}$  is a spherical harmonic.  $\lambda$  is a parameter that is

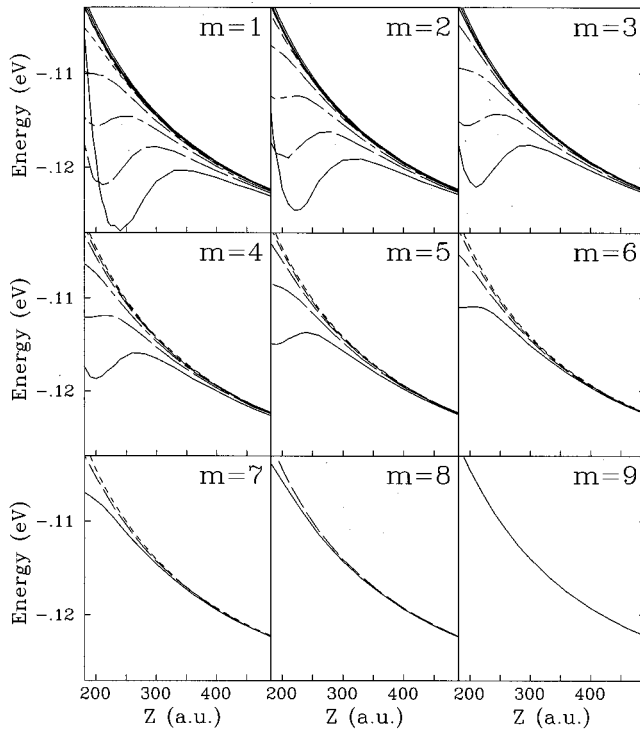


FIG. 7. Calculated energy shifts as a function of distance of  $H(n=10)$ ,  $m=1-9$  outside a jellium surface ( $r_s=2$ ). The different states for each  $m$  are drawn with different dash patterns. The same dashed pattern is used for the corresponding widths shown in Fig. 8.

chosen to optimize the basis set. Since the potential in Eq. (1) has cylindrical symmetry, basis functions with different  $m$  will not interact and the Hamiltonian matrix has a block structure.

The matrix elements are calculated on a multicenter grid. Gauss quadrature is used for efficient numerical integration. The Hamiltonian is then diagonalized. The accuracy of the calculations can be checked by investigating the dependence of the calculated eigenvalues on the parameter  $\alpha$ . For a complete set of basis functions there should be no  $\alpha$  dependence provided  $\alpha > \arctan(k_I/k_R)$ . In typical calculations, basis functions up to  $n=60$  and  $l_{\max}=30$  are included. The accuracy of the resonance calculation is three digits, which is well beyond the accuracy of our surface potential.

### III. RESULTS

In Fig. 3, we show the energy shifts of hydrogenic Rydberg states (with  $m=0$ ) for principal quantum number  $n=7, 8, 9, 10$ , and  $11$ , as a function of distance  $Z$  from the surface. The figure illustrates some of the interesting features of the interaction between Rydberg atoms and metal surfaces. It can be seen that the degeneracy of the atomic orbitals is lifted as the surface is approached. Only the azimuthal quantum number  $m$  remains a good quantum number during the interaction of the atom with the surface. Since the energy difference between states with different principal quantum number is large, the interaction between such states is small. We therefore continue to use the principal quantum number  $n$  when

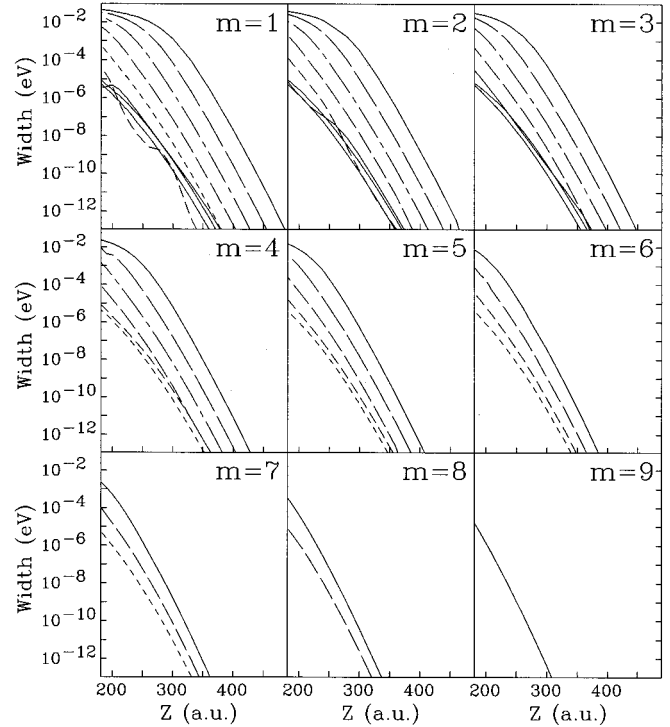


FIG. 8. Calculated widths as a function of distance of  $H(n=10)$ ,  $m=1-9$  states outside a jellium surface ( $r_s=2$ ). The dashed pattern used for the different states are the same as those used in Fig. 7.

referring to the atomic states. For each  $|m|$  and  $n$  there are  $n-|m|$  degenerate atomic orbitals that may hybridize with each other. The interaction with the surface results in the formation of states similar to ‘‘Stark states.’’<sup>23</sup>

For large  $Z$ , all states shift upward with decreasing  $Z$ . This upward shift is approximately equal to  $\Delta\epsilon(Z)=27.2/4Z$  eV. At intermediate distances, some states shift downward with decreasing atom-surface separation. As will be discussed in more detail in Sec. III B, this effect is most pronounced for states oriented toward the surface. The wave function of these states extends into the region  $z < z_c$  in which the surface potential  $\Delta V^{\text{surf}}$  is attractive (see Fig. 1). For the smallest atom-surface separations all atomic levels shift upward. This is caused by the orthogonalization of the atomic states against the surface states when the corresponding overlap becomes finite. It can also be seen from Fig. 3 that the energy separations between states that derive from the  $n$  and  $n \pm 1$  manifolds becomes smaller with increasing  $n$ . For  $H(n=15)$ , some energy levels cross levels deriving both from the  $H(n=14)$  and  $H(n=16)$  manifolds. When this happens, the intra-atomic hybridization can be very pronounced. This will be discussed in a forthcoming paper.<sup>24</sup>

In the following subsections, the calculated energy shifts and broadenings of atomic Rydberg states will be presented for  $H(n=5)$  and  $H(n=10)$  outside an aluminum jellium surface ( $r_s=2$ ).

#### A. $H(n=5)$ states

In Fig. 4 the calculated shifts and broadenings of hydrogen with principal quantum number  $n=5$  are shown for the

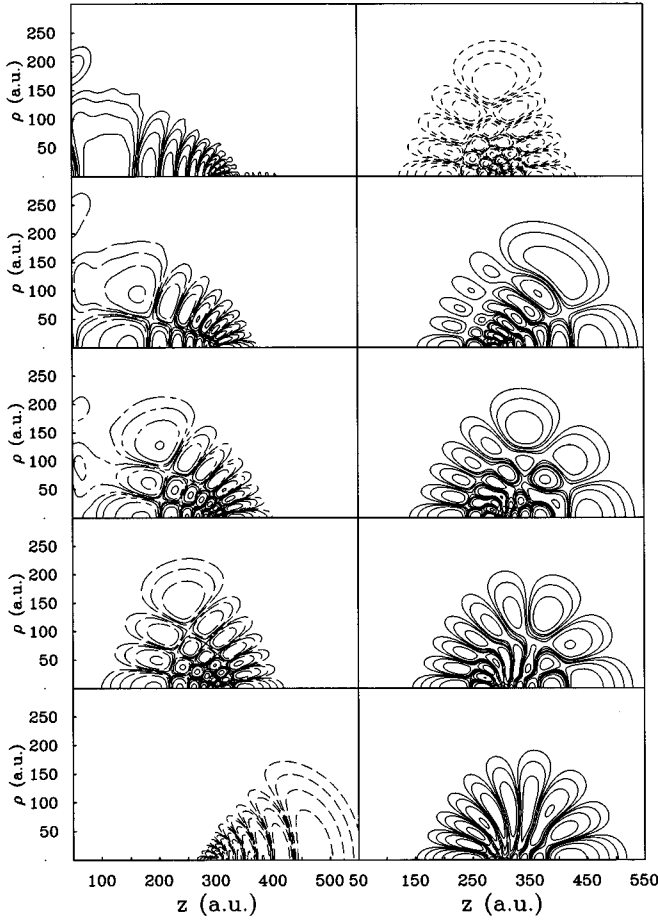


FIG. 9. Contour plot of the probability density  $|\psi(\rho, z)|^2$  for the  $H(n=10)$ ,  $m=0$  states. The hydrogen is placed at  $Z=300$  a.u. The dashed patterns used in each of the subplots are the same as those used in Fig. 6. The contour levels are 0.1, 0.5, 2.5, 12.5, and  $62.5 \times 10^{-7}$  a.u.

five states with  $m=0$ . At very large distances from the surface (not shown), the energies and widths of the atomic orbitals are relatively similar. As the surface is approached, both the energy shifts and broadenings vary with distance in a complex fashion.

A qualitative understanding of the distance dependence of the hybridization can be obtained from simple perturbation theory by considering the asymptotic expansion of  $\Delta V^{\text{surf}}$  for large  $z$  and  $Z$ .<sup>25</sup> A Taylor expansion to the order  $[r/Z]^5$  gives<sup>26,25</sup>

$$\Delta V^{\text{surf}} \rightarrow \left[ \frac{1}{4Z} \right] - \frac{r^2}{16Z^3} - \frac{3r^3}{32Z^4} \cos \theta - \frac{r^2}{16Z^3} \cos^2 \theta - \frac{3r^3}{32Z^4} \cos^3 \theta, \quad (8)$$

where  $\theta$  is the polar angle with respect to an axis perpendicular to the surface. It can be seen from this expression that no linear Stark term is present. As discussed in Sec. II A, this is due to the fact that the surface potential  $\Delta V^{\text{surf}}$  has a maximum at  $z=Z$ . From the expansion Eq. (8), it can be seen that to lowest order the energy shifts of the different atomic or-

bitals  $\langle \phi_{nlm} | \Delta V^{\text{surf}} | \phi_{nlm} \rangle$  will differ by a term inversely proportional to  $Z^3$ . The strongest effect of hybridization on the widths of atomic states is due to the Stark-like third term in Eq. (8). This term mixes symmetric and antisymmetric orbitals resulting in states that can be oriented toward or away from the surface. The matrix element of the Stark term is inversely proportional to  $Z^4$ . Since two orbitals will only hybridize strongly if their matrix element  $\langle \phi_{nlm} | \Delta V^{\text{surf}} | \phi_{nl'm} \rangle$  is larger than their energy separation, the Stark mixing will be very small at large atom-surface separations. As the surface is approached, the Stark matrix elements between the atomic orbitals  $\langle \phi_{nlm} | \Delta V^{\text{surf}} | \phi_{nl \pm 1 m} \rangle$  increase and some of the orbitals start to hybridize, resulting in states that have different orientations with respect to the surface. These states will have very different widths. It can be seen from Fig. 4 that the width of the most short-lived state is several orders of magnitude broader than the most long-lived state. As will be shown in the next section, the most short-lived states are oriented directly toward the surface and the most long-lived states are oriented toward vacuum.

From Fig. 4, it can also be seen that the distance dependence of the widths of some levels is nonexponential. At the atom-surface distances of around  $Z \approx 80$  and  $40$  a.u., the widths of two of the states exhibit kinks. These distances correspond to positions where the Stark matrix element becomes comparable to the energy difference between the corresponding orbitals. This nonmonotonic behavior reflects the formation of hybridized atomic states with a specific orientation with respect to the surface. It can clearly be seen that the width anisotropy increases for distances smaller than these specific  $Z$  points.

In Fig. 5, the energy shifts and widths of the  $m=1-4$  states of  $H(n=5)$  are shown. It can be seen that the interaction is similar to the  $m=0$  case. Since the degeneracy of the atomic levels decreases with increasing azimuthal quantum number, we expect the state orientation effects of intra-atomic hybridization to be smaller with increasing  $m$ . This can clearly be seen from the calculated widths in Fig. 5. As  $m$  becomes larger the anisotropy decreases. We also note that for a given atom-surface separation, the widths of the atomic levels become narrower with increasing  $m$ . This is due to the decrease in overlap between the atomic orbitals and the electronic states of the surface.

### B. $H(n=10)$ states

In Fig. 6, the energies and widths of the ten  $m=0$  states of  $H(n=10)$  are shown as a function of atom-surface separation outside a metal surface. At large distances, the levels are almost degenerate. As the surface is approached, hybridized orbitals are formed and the degeneracy is lifted. Due to the larger spatial extent of the radial wave functions, the interaction with the surface starts at larger distances for the  $H(n=10)$  states than for the  $H(n=5)$  states. The general shape of the energy shifts and broadening of the levels is similar to the  $H(n=5)$  case. Some orbitals have hybridized and formed states with specific orientation with respect to the surface. As would be expected, the effects of orbital hybridization and state orientation are much more pronounced for

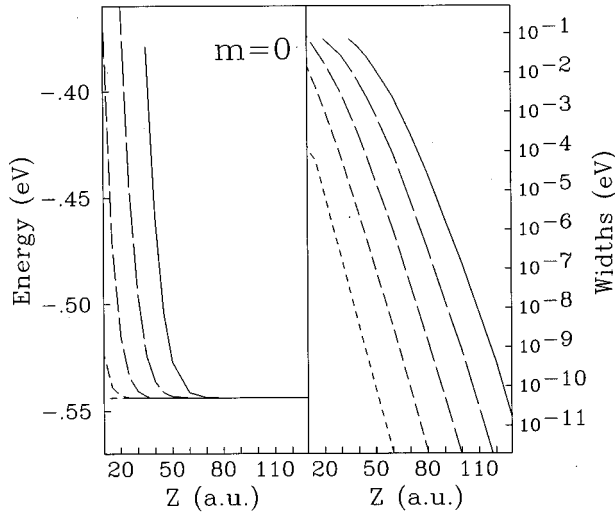


FIG. 10. Calculated energy shifts (left) and widths (right) as a function of distance of  $H(n=5)$ ,  $m=0$  outside a surface modeled using the finite barrier model, Eq. (9). The five different states are drawn with different dashed patterns. The same dashed pattern is used for both the real part and the imaginary part of the energy of the atomic state.

$n=10$  than for  $n=5$ . At a distance of  $Z=300$  a.u., the most long-lived state is more than ten orders of magnitude more long lived than the most short-lived state. From Fig. 5, it can also be seen that the distance dependence of some of the widths is nonexponential. In the interval  $230 \text{ a.u.} > Z > 220 \text{ a.u.}$ , the hybridization between two orbitals increases. This results in the width of one of the states actually decreasing with decreasing atom-surface separation. Similar effects have been seen within all of the  $m=0$  manifolds of hydrogen orbitals with principal quantum number  $5 < n < 18$ .

In Figs. 7 and 8, the calculated energy shift and broadenings of  $H(n=10)$  states with azimuthal quantum numbers  $m=1-9$ . As for  $H(n=5)$ , the hybridization and consequently the effects of state orientation decrease when the degeneracy is decreased. The width of the levels generally decreases with increasing  $m$ .

In order to quantify the effects of hybridization on the orientation of the wave functions of the Rydberg states, the wave functions have been calculated. In Fig. 9, contour plots of the probability density of the ten  $H(n=10)$  states are shown for  $m=0$  for an atom-surface separation of  $Z=300$  a.u.<sup>27</sup> The contours are drawn with the same dashed patterns as were used to show the level shifts and broadenings in Fig. 6. These plots explicitly demonstrate how the surface-induced hybridization results in states with different orientation with respect to the surface. The wave function of the most short lived of the  $H(n=10, m=0)$  states extends directly toward the surface and has negligible weight on the vacuum side of the atomic nucleus. The most long-lived state is oriented toward the vacuum region and has negligible weight on the surface side of the nucleus. The plots in Fig. 9 also illustrate why the energies of certain states shift downward with decreasing atom-surface separation. The surface potential  $\Delta V^{\text{surf}}$  becomes attractive for  $z < z_c$ . For  $Z=300$  a.u.,  $z_c \approx 100$  a.u. From the left panel of Fig. 9, it can be seen

that the four most short-lived states extend well into the region  $z < z_c$ . The five states shown on the right-hand side of Fig. 9 are very similar to each other and show only very small signs of surface interaction. These states correspond to the states with very similar shifts and broadenings drawn with solid and dotted lines in Fig. 6. Since the spatial extent of the wave functions is so similar, one can understand why the energy shifts and broadenings of these states are so similar. For smaller atom-surface separations these states will also start to hybridize, resulting in states with more pronounced orientations with respect to the surface. When this happens, the differences between their widths also increase.

#### IV. DISCUSSION

It is not possible to directly compare the present results with the results from perturbation theory.<sup>10,12</sup> The perturbative approach neglects the hybridization between the atomic orbitals. As was demonstrated in the present calculation, the hybridization of the atomic orbitals results in states with shifts and broadenings that vary greatly from each other. A comparison between widths calculated using the complex scaling method and widths calculated using the perturbative approach for  $H(n=2)$  and  $H(n=3)$  adopting a Stark representation have shown reasonable agreement.<sup>28</sup>

In calculating the energy shift and broadenings of atomic levels near surfaces it is crucial to employ an accurate description of the surface. In Fig. 10, the energy shifts and broadenings of the five  $H(n=5, m=0)$  states are shown as a function of atom-surface separation outside a surface modeled using the finite barrier model (FBM), i.e.,

$$\Delta V^{\text{surf}}(z) = V_0 \Theta(-z). \quad (9)$$

The depth  $V_0$  is chosen as the bulk value of the jellium potential for  $r_s=2$ , i.e.,

$$V_0 = \lim_{z \rightarrow -\infty} V_0^s(z) = -16.4 \text{ eV}. \quad (10)$$

It can clearly be seen that both the shifts and broadening of the atomic levels are very different from those in Fig. 4. For the FBM, the levels never show any downshift. This is because the interaction between the Rydberg levels and the surface is dominated by the orthogonalization energy and hybridization between the atomic level and the bound states of the surface. Since the energies of the surface states are lower than the Rydberg states the interaction with the surface results in an upward shift of the atomic states. From Fig. 10, it can also be seen that the anisotropy of the widths is much larger for the FBM than for the density-functional potential. This is because the FBM potential results in larger hybridization and more efficient alignment of the atomic orbitals. Since the FBM potential is zero outside the surface, the energy shifts of the atomic orbitals are very small. The overlap matrix element is larger than the energy shifts even at large atom-surface separation resulting in an efficient hybridization and alignment of the atomic states.

These results show that the hybridization of the Rydberg orbitals depends sensitively on the details of the surface potential. When calculating the energy shifts and broadenings of atomic Rydberg levels it is therefore important to employ a realistic surface potential.

## V. CONCLUSIONS

The energy shifts and broadenings of atomic Rydberg states outside a metal surface have been calculated as a function of atom-surface separation. It was found that the surface-induced hybridization of the atomic orbitals results in states with different orientations with respect to the surface. For a given atom-surface separation, the widths of these states can differ by many orders of magnitude. The hybridization is found to be sensitive to the details of the surface

potential. This calculation thus shows that for an accurate description of the energy shifts and broadenings of atomic Rydberg levels outside a metal surface it is crucial to employ a realistic model of the surface.

## ACKNOWLEDGMENTS

Valuable discussions with Dr. F. B. Dunning and Dr. N. J. Halas are acknowledged. This work is supported by the National Science Foundation under Grant No. DMR-9521444.

- 
- <sup>1</sup>F. Aumayr and H. P. Winter, *Comments At. Mol. Phys.* **29**, 275 (1994).
- <sup>2</sup>S. Y. Leung, N. H. Tolk, W. Heiland, J. C. Tully, J. S. Kraus, and P. Hill, *Phys. Rev. A* **18**, 447 (1978).
- <sup>3</sup>H. Steininger, B. Willerding, K. Snowdon, N. H. Tolk, and W. Eckstein, *Nucl. Instrum. Methods Phys. Res. Sect. B* **2**, 484 (1984).
- <sup>4</sup>J. Neumann, S. Schubert, U. Imke, P. Varga, and W. Heiland, *Europhys. Lett.* **3**, 859 (1987).
- <sup>5</sup>S. Kupryanov, *Pis'ma Zh. Éksp. Teor. Fiz.* **5**, 245 (1967) [*JETP Lett.* **5**, 197 (1967)].
- <sup>6</sup>C. Fabre, M. Gross, J. M. Ramond, and S. Haroche, *J. Phys. B* **16**, L671 (1983).
- <sup>7</sup>C. A. Kocher and C. R. Taylor, *Phys. Lett. A* **124**, 68 (1987).
- <sup>8</sup>D. F. Gray, Z. Zheng, K. A. Smith, and F. B. Dunning, *Phys. Rev. A* **38**, 1601 (1988).
- <sup>9</sup>A. V. Chaplik, *Zh. Éksp. Teor. Fiz.* **54**, 332 (1968) [*Sov. Phys. JETP* **27**, 178 (1968)].
- <sup>10</sup>U. Wille, *Nucl. Instrum. Methods Phys. Res. Sect. B* **67**, 132 (1992).
- <sup>11</sup>U. Wille, *Surf. Sci.* **307**, 874 (1993).
- <sup>12</sup>U. Wille, *Phys. Rev. B* **50**, 1888 (1994).
- <sup>13</sup>P. Nordlander and J. C. Tully, *Phys. Rev. B* **42**, 5564 (1990).
- <sup>14</sup>N. D. Lang and W. Kohn, *Phys. Rev. B* **1**, 4555 (1970).
- <sup>15</sup>O. Gunnarsson and R. O. Jones, *Phys. Scr.* **21**, 394 (1980).
- <sup>16</sup>S. Ossicini, C. M. Bertoni, and P. Gies, *Europhys. Lett.* **1**, 661 (1986).
- <sup>17</sup>N. D. Lang and W. Kohn, *Phys. Rev. B* **7**, 3541 (1973).
- <sup>18</sup>L. Hedin and B. I. Lundqvist, *J. Phys. C* **4**, 2064 (1971).
- <sup>19</sup>W. P. Reinhardt, *Annu. Rev. Phys. Chem.* **33**, 223 (1982).
- <sup>20</sup>B. R. Junker, *Adv. At. Mol. Phys.* **18**, 207 (1982).
- <sup>21</sup>P. Nordlander and N. Lang, *Phys. Rev. B* **44**, 13 681 (1991).
- <sup>22</sup>P. Nordlander, *Phys. Rev. B* **46**, 2584 (1992).
- <sup>23</sup>P. Nordlander and J. C. Tully, *Phys. Rev. Lett.* **61**, 990 (1988).
- <sup>24</sup>P. Nordlander and F. B. Dunning (unpublished).
- <sup>25</sup>A. G. Borisov, D. Teillet-Billy, and J. P. Gauyacq, *Nucl. Instrum. Methods Phys. Res. Sect. B* **78**, 49 (1993).
- <sup>26</sup>L. W. Bruch and T. W. Ruijgrok, *Surf. Sci.* **79**, 509 (1979).
- <sup>27</sup>The wave function of a resonance state diverges asymptotically. A qualitative representation of the wave function is obtained by analytically continuing the resonance wave function to  $\theta=0$ . The wave function so obtained is normalizable.
- <sup>28</sup>U. Wille, *Nucl. Instrum. Methods Phys. Res. Sect. B* **79**, 132 (1993).